Dynamics of the *N*-link pendulum: a fractional perspective

António M. Lopes and J. A. Tenreiro Machado

ABSTRACT
This paper addresses the dynamics of an *N*-link planar pendulum in the perspective of fractional calculus. The proposed methodology leads to a novel point of view for signal propagation as a time-space wave within the system mechanical structure. Numerical simulations show the effectiveness of the approach both for signal visualisation and limit cycle detection.

KEYWORDS
N-link pendulum; fractional calculus; dynamical systems; signal propagation; limit cycle

1. Introduction

Known for their rich dynamics, pendular systems (PS) have been widely used for modelling and as benchmark systems in many areas, namely long-chain molecular physics (Mezić, 2006; Vesely, 2013), control theory (Boubaker, 2013; Kurdekar & Borkar, 2013; Larcombe, 1992), robotics (Ali, Motoi, Heerden, & Kawamura, 2013; Brisilla & Sankaranarayanan, 2015), biomechanics (Barin, 1992; Schiehlen, 2014), building structures (Housner, 1963; Zayas, Low, & Mahin, 1990), chaos and nonlinear dynamics (Gmiterko & Grossman, 2010; Hedrih, 2008; Lobas, 2005; Yu & Bi, 1998), among others (Baker & Blackburn, 2005; Jadlovská, Sarnovskỳ, Vojtek, & Vošček, 2015).

PS have been studied in the perspective of developing models of increasing complexity with the number of links, by means of computational packages (Gmiterko & Grossman, 2010; Rivas-Cambero & Sausedo-Solorio, 2012). Another point of view is the analysis of the complex dynamics emerging in PS with a large number of links (Awrejcewicz et al., 2008). In all cases, the popularity of PS is due to their seminal properties, revealing phenomena ubiquitous in natural and man-made systems (Boubaker, 2013). Despite the existing models being able to deal with PS of arbitrary number of links, the lack of general tools for dynamical analysis and performance visualisation is recognised (Rivas-Cambero & Sausedo-Solorio, 2012).

In this paper, we propose a methodology inspired in fractional calculus (FC) to explore the dynamics of an *N*-link planar pendulum in the line of thought of signal propagation and limit cycle prediction. First, we use the Lagrange–Euler formulation to obtain the system model as a set of general equations, easily implementable with present-day symbolic computational packages. Second, we explore the dynamics and the tools of FC to visualise signal propagation within the system mechanical structure. Third, we address the emergence of limit cycles and their prediction by means of an harmonic analysis. The results of several numerical experiments are discussed. The proposed methodology leads to a novel perspective for signal propagation as time-space waves within the PS.

Having these ideas in mind, the paper is organised as follows. In Sections 2 and 3, we present the main mathematical tools for processing data and we derive the general model of the *N*-link pendulum. In Section 4, we simulate the system dynamics, proposing a methodology for visualising signal-wave propagation. In Section 5, we analyse the complexity of limit cycles revealed by the PS. Finally, in Section 6, we outline the main conclusions.

2. Mathematical tools

In this section, we present the main mathematical tools used during the data processing. Hence, in Sections 2.1 and 2.2, we address briefly the concepts of fractional-order 'differintegral' and fractional power of a square matrix, respectively.

2.1 Fractional-order derivatives and integrals

FC generalises the concepts of derivative and integral to non-integer orders. During the last decades, FC was found to play a fundamental role in modelling

many important physical phenomena and emerged as an important tool in the area of dynamical systems with complex behaviour (Baleanu, Diethelm, Scalas, & Trujillo, 2012; Ionescu, 2013; Kenneth & Ross, 1993; Lopes & Machado, 2014; Lopes, Machado, Pinto, & Galhano, 2013; Luo & Chen, 2012; Mainardi, 2010; Sheng, Chen, & Qiu, 2011; Silva, Machado, & Lopes, 2004).

Several definitions of fractional derivative and integral have been proposed (de Oliveira & Machado, 2014; Machado, Kiryakova, & Mainardi, 2011; Valério, Trujillo, Rivero, Machado, & Baleanu, 2013). We recall here the Grünwald–Letnikov fractional 'differintegral' operator of order $\alpha \in \mathbb{R}$, ${}_aD_t^\alpha$, given by (Petras, 2011)

$$ {}_aD_t^\alpha f(t) = \lim_{h\to 0} h^{-\alpha} \sum_{m=0}^{[\frac{t-a}{h}]} (-1)^m \binom{\alpha}{m} f(t-mh) \quad (1) $$

where $[\,\cdot\,]$ denotes the integer part, h is the time increment, and $\{t, a\} \in \mathbb{R}$ are the upper and lower limits of the 'differintegral' operation, respectively.

Equation (1) can be easily approximated numerically by (Dorčák, 1994; Podlubny, 1999)

$$ \begin{aligned} {}_aD_t^\alpha f(t) &\approx {}_{(t-L)}D_t^\alpha f(t) \\ &= T^{-\alpha} \sum_{m=0}^{N(t)} (-1)^m \binom{\alpha}{m} f(t-mT) \\ &= T^{-\alpha} \sum_{m=0}^{N(t)} c_m^{(\alpha)} f(t-mT) \end{aligned} \quad (2) $$

where T is the sampling period, L corresponds to the 'memory length', and $N(t) = \min\{[t/h], [L/h]\}$.

The binomial coefficients $c_m^{(\alpha)}$ are given by (Dorčák, 1994)

$$ c_m^{(\alpha)} = \left(1 - \frac{1+\alpha}{m}\right) c_{m-1}^{(\alpha)}, \quad c_0^{(\alpha)} = 1 \quad (3) $$

Parameter L should be chosen using the following criterion:

$$ L \geq \frac{1}{\delta_0^2 \Gamma(\alpha)} \quad (4) $$

where δ_0 is the maximum admissible normalised error, given by

$$ \delta_0 = \frac{|{}_aD_t^\alpha f(t) - {}_{(t-L)}D_t^\alpha f(t)|}{M}, \quad M = \max_{[0,\infty]} |f(t)| \quad (5) $$

2.2 Fractional power of a square matrix

The calculation of the pth power of a square $n \times n$ real matrix $\mathbf{A}$, where p is a real or complex value, arises in applications such us Markov chain models in finance and health care (Charitos, de Waal, & van der Gaag, 2008; Israel, Rosenthal, & Wei, 2001), fractional differential equations, nonlinear matrix equations, and computation (Bini, Higham, & Meini, 2005; Fiori, 2008).

Several authors have investigated algorithms for computing the pth power of matrices. In Higham (2008) are presented the Schur, Newton, and inverse Newton methods. The Schur–Newton and Schur–Padé algorithms are discussed in Higham and Lin (2011). Some of these methods impose additional conditions on the matrix $\mathbf{A}$.

In this subsection, we recall a reliable method for computing $\mathbf{A}^p$, $p \in \mathbb{C}$, based on the eigenvalue decomposition (Machado, Lopes, Duarte, Ortigueira, & Rato, 2014).

Given a real square $n \times n$ matrix $\mathbf{A}$, with the eigenvalues λ_i (real or complex) and the corresponding eigenvectors $\mathbf{v}_i$, $1 \leq i \leq n$, $\mathbf{v}_i \neq \mathbf{0}$, there is the well-know relation

$$ \mathbf{A}\mathbf{v}_i = \lambda_i \mathbf{v}_i \quad (6) $$

It can be easily shown by induction on k that

$$ \mathbf{A}^k \mathbf{v}_i = \lambda_i^k \mathbf{v}_i \quad (7) $$

for all positive integers k.

Let us now consider the generalisation of Equation (7) to the case $k = \frac{1}{p}$, $p \in \mathbb{Z}$, $p \neq 0$. This yields

$$ \mathbf{A}^{\frac{1}{p}} \mathbf{v}_i = \lambda_i^{\frac{1}{p}} \mathbf{v}_i \quad (8) $$

The p root of the matrix $\mathbf{A}$ should be defined as a matrix $\mathbf{B}$ such that $\mathbf{B}^p = \mathbf{A}$. Therefore, $\mathbf{B} = \mathbf{A}^{\frac{1}{p}}$ satisfies Equation (8) for all eigenvalues and the corresponding eigenvectors (Arias, Gutierrez, & Pozo, 1990; Astin, 1967; Bini et al., 2005; Waugh & Abel, 1967). Expression (8) can be written as

$$ \mathbf{B}\mathbf{v}_i = \lambda_i^{\frac{1}{p}} \mathbf{v}_i \quad (9) $$

Matrix $\mathbf{B}$ can be determined by solving the linear system:

$$ \mathbf{B}\left[\mathbf{v}_1|\mathbf{v}_2|\ldots|\mathbf{v}_n\right] = \left[\lambda_1^{\frac{1}{p}}\mathbf{v}_1|\lambda_2^{\frac{1}{p}}\mathbf{v}_2|\ldots|\lambda_n^{\frac{1}{p}}\mathbf{v}_n\right] \quad (10) $$

$$ \mathbf{B} = \left[\lambda_1^{\frac{1}{p}}\mathbf{v}_1|\lambda_2^{\frac{1}{p}}\mathbf{v}_2|\ldots|\lambda_n^{\frac{1}{p}}\mathbf{v}_n\right] \cdot \left[\mathbf{v}_1|\mathbf{v}_2|\ldots|\mathbf{v}_n\right]^{-1} \quad (11) $$

Obviously, different sort of eigenvalues may produce distinct results, while negative eigenvalues of $\mathbf{A}$ result in complex elements of $\mathbf{A}^p$. The main limitation is the computational burden for calculating the matrix's spectrum.

Using the identity $\lambda_i^j = e^{j \ln \lambda_i} = \cos(\ln \lambda_i) + j \sin(\ln \lambda_i)$, $j = \sqrt{-1}$, it is possible to extend the determination of $\mathbf{A}^p$ to complex powers, $p \in \mathbb{C}$.

3. Dynamics of the *N*-link pendulum

We consider the N-link planar pendulum shown in Figure 1. The kth link, $k = 1, ..., N$, is a rigid body with length l_k and punctual mass m_k, concentrated at a distance r_k from the link base point. The link angular position, θ_k, is measured with reference to the axis of link $k-1$, except for θ_1 that is measured with reference to the negative y-axis of the fixed Cartesian frame xy.

For computing the dynamic model of the pendulum, we use the Lagrange–Euler formulation, given by

$$\frac{d}{dt}\frac{\partial L}{\partial \dot{\theta}_k} - \frac{\partial L}{\partial \theta_k} = T_k \tag{12a}$$

$$L = K - P \tag{12b}$$

where, L is the Lagrangian, K and P denote the system kinetic and potential energies, respectively, T_k is the torque acting on link k, at the link base point, and t is time.

The energies K and P can be written as

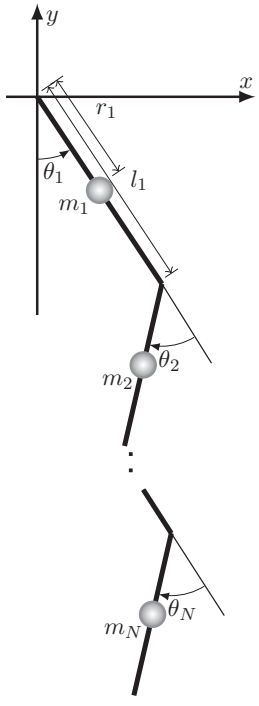

Figure 1. The *N*-link planar pendulum.

$$K = \sum_{k=1}^{N} \frac{1}{2} m_k \times \left[\left(\sum_{i=1}^{k-1} l_i \cos(\theta_{i,i-1}) \dot{\theta}_{i,i-1} + r_k \cos(\theta_{k,k-1}) \dot{\theta}_{k,k-1} \right)^2 + \left(\sum_{i=1}^{k-1} l_i \sin(\theta_{i,i-1}) \dot{\theta}_{i,i-1} + r_k \sin(\theta_{k,k-1}) \dot{\theta}_{k,k-1} \right)^2 \right] \tag{13}$$

$$P = -g \sum_{k=1}^{N} m_k \left[\sum_{i=1}^{k-1} l_i \cos(\theta_{i,i-1}) + r_k \cos(\theta_{k,k-1}) \right] \tag{14}$$

where g represents the gravitational acceleration, $\theta_{j,j-1} = \theta_j + \theta_{j-1}$, $j = \{i, k\}$, and $\theta_0 = 0$.

Substituting Equations (13) and (14) into Equation (12), we can write the pendulum inverse dynamical model in the matrix form:

$$\mathbf{I}(\theta)\ddot{\theta} + \mathbf{N}(\theta, \dot{\theta}) + \mathbf{G}(\theta) = \mathbf{T} \tag{15}$$

where $\mathbf{I}(\theta)$ denotes the $N \times N$ dimensional matrix of inertia, $\mathbf{N}(\theta, \dot{\theta})$ and $\mathbf{G}(\theta)$ represent the $N \times 1$ dimensional vectors of Coriolis plus centripetal and gravitational terms, respectively, and $\mathbf{T}$ is the $N \times 1$ torque vector acting upon the pendulum links. The inverse model (15) may be used within certain feedforward control schemes (Machado & de Carvalho, 1989; Machado, de Carvalho, & Galhano, 1993), while the direct model, represented in Figure 2 as a block diagram, is required for simulation (Lewis, Dawson, & Abdallah, 2004; Slotine, 1985; Spong & Vidyasagar, 2008).

Model (15) can be calculated in analytic form, for an arbitrary number of links, by symbolic computational software packages (Char, Fee, Geddes, Gonnet, & Monagan, 1986; Moore, 2014; Wolfram, 2000).

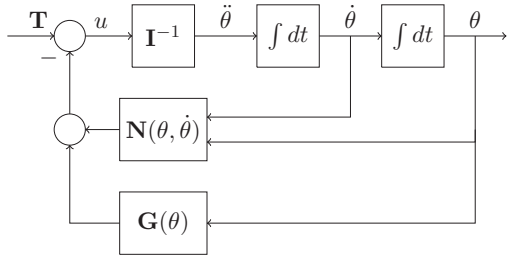

Figure 2. Diagram of the *N*-link pendulum direct dynamics.

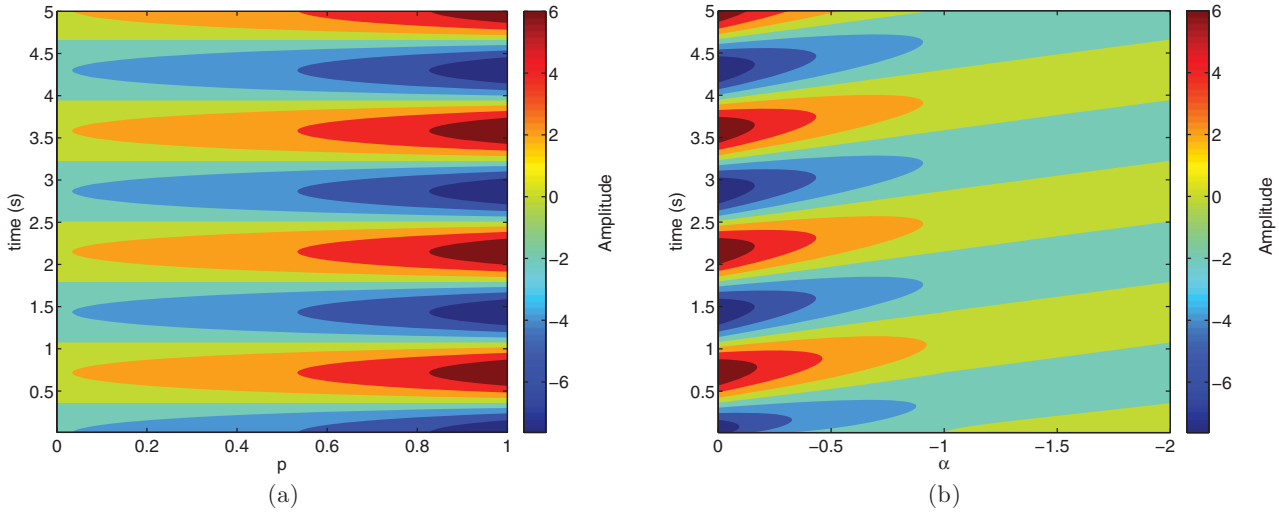

Figure 3. Forward path signal propagation for the 1-link planar pendulum: (a) ϑ_1; (b) ψ_1. The pendulum parameters are $l_1 = 1$, $m_1 = 1$, $r_1 = 0.5$, and the initial conditions are $\theta = 0.4$, $\dot{\theta} = 0$.

4. Numerical simulation and computer visualisation

In this section, we visualise the signal propagation across the forward path of the block diagram of Figure 2. The propagation in the feedback path, either joining N and G, or separately, is straightforward using the method proposed in the sequel. Several numerical experiments showed that the visualisation across N and G does not add any significant information and, therefore, for the matter of reducing space, in the sequel we focus our attention mainly in the direct path. We start by calculating the travelling signal, $\vartheta = (\mathbf{I}^{-1})^p \cdot \mathbf{u}$, $p \in [0, 1]$, from $\mathbf{u}$ towards $\ddot{\theta}$. Therefore, for $p = 0$, we have $\vartheta = \mathbf{u}$, while for $p = 1$, we obtain $\vartheta = \ddot{\theta}$. This is accomplished by means of the fractional power of a square matrix operator (11).

We then determine and visualise the signal, $\psi = {}_aD_t^{\alpha}\,\ddot{\theta}(t)$, $\alpha \in [-2, 0]$, travelling from $\ddot{\theta}$ towards θ. Therefore, for $\alpha = 0$, we have $\psi = \ddot{\theta}$, while for $\alpha = -2$, we obtain $\psi = \theta$. This means that we successively integrate the acceleration, $\ddot{\theta}$, by means of the fractional-order 'differintegral' operator, until we get the link's position, θ. This scheme may be considered as a pure mathematical and numerical approach. In fact, the obtained results are to be interpreted as a new visualisation concept inspired in the FC. Therefore, obtaining a physical meaning is not the goal of this study, rather than to open a new research procedure to the classical integer modus operandi.

For supporting the study, we analyse in the sequel the pendulum dynamics for $N = \{1, 2, 3, 4\}$. Furthermore, in order to facilitate the comparison and the interpretation of the results, we impose the constraints $m_k = l_k = \frac{1}{N}$ and $r_k = \frac{l_k}{2}$ on the pendulum parameters. By other words, we adopt PS with invariant total length and mass. For all experiments, we consider the unforced case with a given set of initial conditions on θ and $\dot{\theta}$.

Figures 3 and 4 depict the signal propagation along the forward path for the 1- and 2-link pendula, respectively. The corresponding initial conditions are $\theta = \{0.4\}$, $\dot{\theta} = \{0\}$, and $\theta = \{0.4, 0\}$, $\dot{\theta} = \{0, 0\}$. Despite the uncountable possibilities, these values illustrate well the system dynamics, while other options lead to similar results.

Figures 5 and 6 show the results obtained for $N = \{3, 4\}$, with the initial conditions $\theta = \{0.4, 0, 0\}$, $\dot{\theta} = \{0, 0, 0\}$, and $\theta = \{0.4, 0, 0, 0\}$, $\dot{\theta} = \{0, 0, 0, 0\}$, respectively. As said before, these values illustrate well the system dynamics, while other options lead to similar results. Moreover, for both pendula, we opt for depicting just the signals corresponding to the first link. In fact, while for all links the results are similar, the first one often unveils richer dynamics.

We observe a continuous variation of the signals. Furthermore, we verify the nonlinear action of the inertia matrix, with the emergence of multiple harmonics, particularly visible when p is close to one. On the other hand, it is noticeable that the waves have a propagation along the x-axis merely for the inertia, while they reveal a diagonal evolution along the acceleration-to-position integration path due to the involved memory effect.

5. Limit cycles

In this section, we study the limit cycles of the N-link pendulum.

In general, the link's positions, θ, of the unforced pendulum are periodic, but include higher harmonics

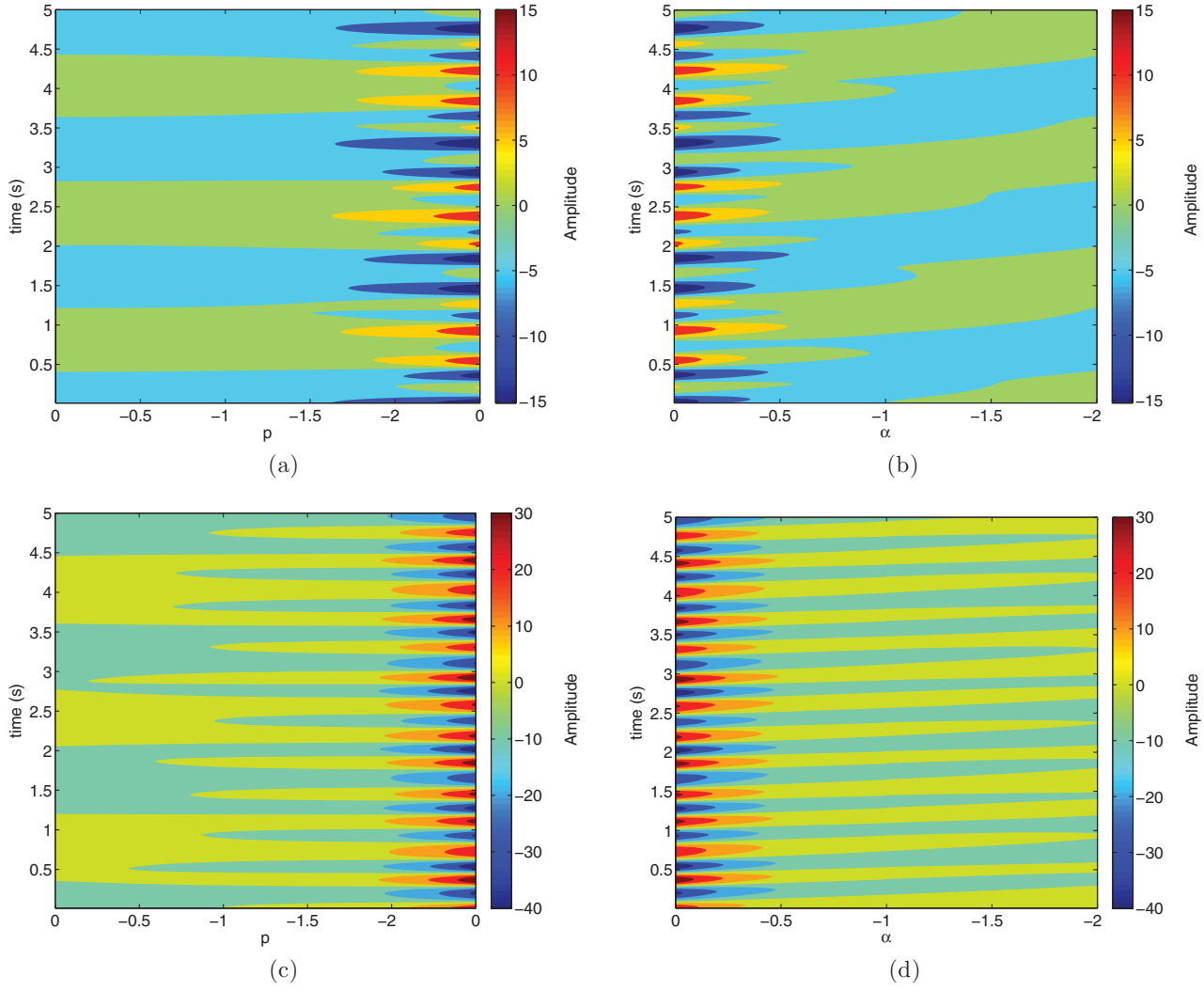

Figure 4. Forward path signal propagation for the 2-link planar pendulum: (a) ϑ_1; (b) ψ_1; (c) ϑ_2; (d) ψ_2. The pendulum parameters are $\{l_1, l_2\} = \{0.5, 0.5\}$, $\{m_1, m_2\} = \{0.5, 0.5\}$, $\{r_1, r_2\} = \{0.25, 0.25\}$, and the initial conditions are $\theta = \{0.4, 0\}$, $\dot{\theta} = \{0, 0\}$.

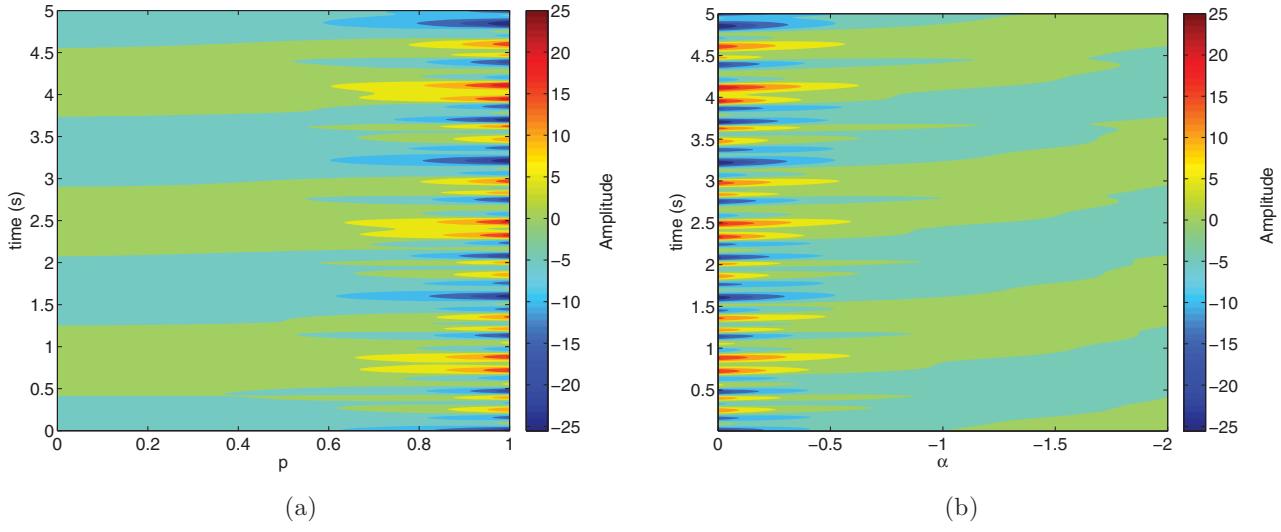

Figure 5. Forward path signal propagation for the first link of the 3-link planar pendulum: (a) ϑ_1; (b) ψ_1. The pendulum parameters are $\{l_1, l_2, l_3\} = \{1/3, 1/3, 1/3\}$, $\{m_1, m_2, m_3\} = \{1/3, 1/3, 1/3\}$, $\{r_1, r_2, r_3\} = \{1/6, 1/6, 1/6\}$, and the initial conditions are $\theta = \{0.4, 0, 0\}$, $\dot{\theta} = \{0, 0, 0\}$.

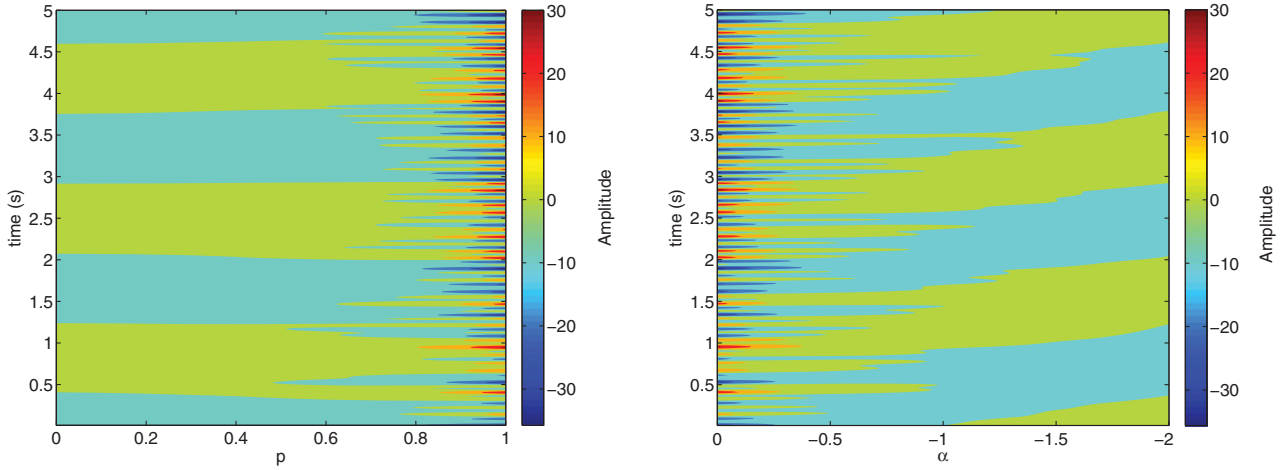

Figure 6. Forward path signal propagation for the first link of the 4-link planar pendulum: (a) ϑ_1; (b) ψ_1. The pendulum parameters are $\{l_1, l_2, l_3, l_4\} = \{0.25, 0.25, 0.25, 0.25\}$, $\{m_1, m_2, m_3, m_4\} = \{0.25, 0.25, 0.25, 0.25\}$, $\{r_1, r_2, r_3, r_4\} = \{0.125, 0.125, 0.125, 0.125\}$, and the initial conditions are $\theta = \{0.4, 0, 0, 0\}$, $\dot{\theta} = \{0, 0, 0, 0\}$.

besides their fundamental frequency. Thus, according to the Fourier series decomposition, we have (Mitra & Kuo, 2006; Papoulis, 1977)

$$\theta_k(t) = A_0 + \sum_{n=1}^{\infty} [Y_n \sin(n\omega t + \phi_n)] \tag{16}$$

where A_0 is a constant, and Y_n and ϕ_n are the amplitude and the phase shift of the nth harmonic, respectively.

We assume that only the fundamental frequency $A_0 + Y_1 \sin(\omega t + \phi_1)$ of the output is relevant. This is usually valid, not only because the higher harmonics have small amplitudes, but also because any physical system is often a 'low-pass filter' attenuating even further the higher harmonics (Slotine et al., 1991).

We start considering that the angular displacements of all links follow the harmonic functions:

$$\theta_k(t) = A_k \cos(\omega t) \tag{17}$$

This assumption is based on the experimental observation that all links oscillate with the same frequency, ω, and in phase with each other (or, at most, in phase opposition).

We then substitute Equation (17) (and its time derivatives) into Equation (15) and use the following expressions (Abramowitz & Stegun, 1965):

$$\cos(x \sin\phi) = J_0(x) + 2\sum_{n=1}^{\infty} J_{2n}(x) \cos(2n\phi) \tag{18}$$

$$\sin(x \sin\phi) = 2\sum_{n=0}^{\infty} J_{2n+1}(x) \sin[(2n+1)\phi] \tag{19}$$

where J_q represents the Bessel function of the first kind and order $q \in \mathbf{N}_0$.

Considering the unforced pendulum, $\mathbf{T} = 0$, and neglecting all higher harmonics, we obtain the following set of N equations:

$$\begin{cases} \Phi_1(A_1, A_2, ..., A_N, \omega) = 0 \\ ... \\ \Phi_N(A_1, A_2, ..., A_N, \omega) = 0 \end{cases} \tag{20}$$

so that its solution represent the amplitude and frequency of the limit cycle.

In the sequel, we analyse the limit cycles of the four pendula, $N = \{1, 2, 3, 4\}$, already presented in Section 4.

For $N = \{1, 2\}$, Equation (20) yields Equations (21) and (22), respectively:

$$\Phi_1(A_1, \omega) = 2gJ_1(A_1) - A_1\omega^2 r_1 = 0 \tag{21}$$

$$\begin{cases} \Phi_1(A_1, A_2, \omega) = 2A_1A_2J_1(A_2)w^2l_1m_2r_2 \\ \quad +2A_1A_2J_3(A_2)w^2l_1m_2r_2 \\ \qquad +A_2^2J_1(A_2)w^2l_1m_2r_2 + A_2^2J_3(A_2)w^2l_1m_2r_2 \\ \qquad +4A_1J_0(A_2)w^2l_1m_2r_2 - 4A_1J_2(A_2)w^2l_1m_2r_2 \\ \qquad +2A_2J_0(A_2)w^2l_1m_2r_2 - 2A_2J_2(A_2)w^2l_1m_2r_2 \\ \qquad +2A_1w^2l_1^2m_2 + 2A_1w^2m_1r_1^2 + 2A_1w^2m_2r_2^2 \\ \qquad +2A_2w^2m_2r_2^2 - 4J_1(A_1)gl_1m_2 - 4J_1(A_1)gm_1r_1 \\ \qquad -4J_1(A_1 + A_2)gm_2r_2 = 0 \\ \Phi_2(A_1, A_2, \omega) = A_1^2J_1(A_2)w^2l_1 + A_1^2J_3(A_2)w^2l_1 \\ \qquad -2A_1J_0(A_2)w^2l_1 + 2A_1J_2(A_2)w^2l_1 - 2A_1w^2r_2 \\ \quad -2A_2w^2r_2 \\ \qquad +4J_1(A_1 + A_2)g = 0 \end{cases} \tag{22}$$

where Φ_k correspond to the links $k = \{1, 2\}$.

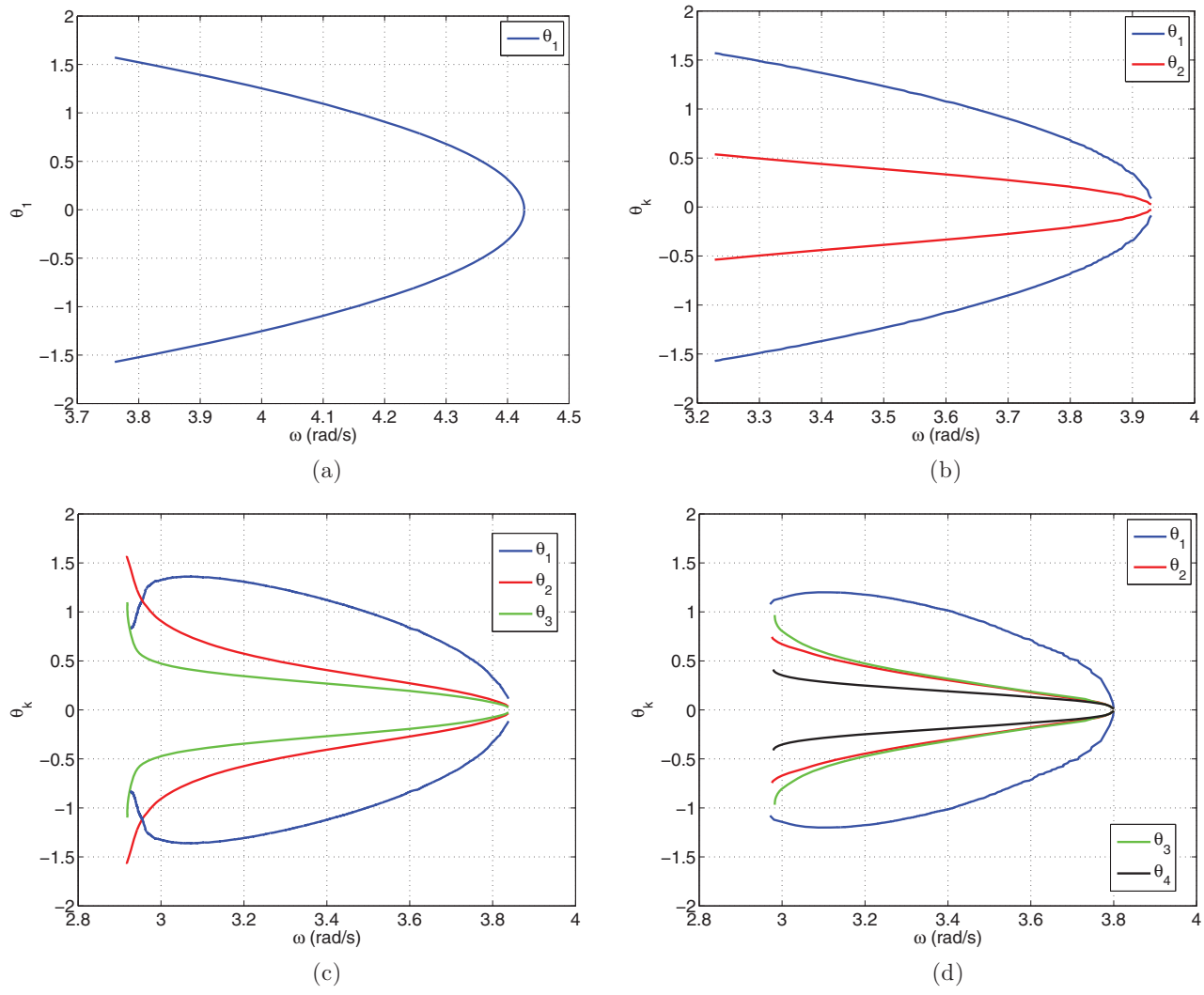

Figure 7. Limit cycle amplitude and frequency of the pendula, $\Phi(A_1, A_2, ..., A_N, \omega) = 0$: (a) $N = 1$; (b) $N = 2$; (c) $N = 3$; (d) $N = 4$.

It should be noted that for higher numbers of links, the equations $\Phi_k = 0$ can be calculated by means of symbolic computational packages. However, since their complexity increases significantly with N and there are no relevant distinct dynamical effects, they are not presented.

Figure 7 depicts $\Phi(A_1, A_2, ..., A_N, \omega) = 0$ for the pendula with $N = \{1, 2, 3, 4\}$. We observe that the charts are symmetrical relatively to the amplitude. On the other hand, we verify that as frequency gets higher, the amplitudes become smaller. While these phenomena are known, it is interesting to observe that the charts tend to approximate to a stable value as N increases.

In conclusion, the fractional perspective leads to a visualisation of the signal wave propagation along the mechanical structure and the results are in accordance with the prediction of limit cycles be means of an harmonic approximation.

6. Conclusions and future work

A methodology inspired in FC was proposed to explore the dynamics of an N-link planar pendulum. First, we used the Lagrange–Euler formulation to obtain the system dynamical model as a set of general equations that can be easily implemented in most symbolic computation software packages. Second, we explored the structure of the dynamical model and the tools of FC to visualise the signal propagation along the system structure. Third, we addressed the presence of limit cycles. The proposed methodology led to a novel view point for signal propagation as time-space waves within the system structure. The dynamics of PS was the primary goal of this study, but new possibilities emerge such as, for example, the application of the method in control schemes. Therefore, future work will tackle such research avenues, since we can now consider the signal propagation both along the computational and mechanical structures.

Disclosure statement

The authors declare that there are no conflicts of interest.

ORCID

António M. Lopes http://orcid.org/0000-0001-7359-4370
J. A. Tenreiro Machado http://orcid.org/0000-0003-4274-4879

References

Abramowitz, M., & Stegun, I.A. (Eds.). (1965). *Handbook of mathematical functions with formulas, graphs, and mathematical tables*. New York, NY: Dover.

Ali, F., Motoi, N., Heerden, K., & Kawamura, A. (2013). Ground reaction force reduction of biped robot for walking along a step with dual length linear inverted pendulum method. *Journal of Robotics and Mechatronics, 25*(1), 220–231.

Arias, A., Gutierrez, E., & Pozo, E. (1990). Binomial theorem applications in matrix fractional powers calculation. *Transportation Engineering, 18*(1–2), 75–79.

Astin, J. (1967). Extension of the formula for the Nth power of a square matrix to negative and fractional values of N. *The Mathematical Gazette, 51*(377), 228–232.

Awrejcewicz, J., Supeł, B., Lamarque, C.-H., Kudra, G., Wasilewski, G., & Olejnik, P. (2008). Numerical and experimental study of regular and chaotic motion of triple physical pendulum. *International Journal of Bifurcation and Chaos, 18*(10), 2883–2915.

Baker, G.L., & Blackburn, J.A. (2005). *The pendulum: A case study in physics*. Oxford: Oxford University Press.

Baleanu, D., Diethelm, K., Scalas, E., & Trujillo, J.J. (2012). *Fractional calculus: Models and numerical methods* (Vol. 3). Singapore: World Scientific.

Barin, K. (1992). Dynamic posturography: Analysis of error in force plate measurement of postural sway. *Engineering in Medicine and Biology Magazine, IEEE, 11*(4), 52–56.

Bini, D., Higham, N., & Meini, B. (2005). *Algorithms for the matrix pth root. Numerical Algorithms, 39*(4), 349–378.

Boubaker, O. (2013). The inverted pendulum benchmark in nonlinear control theory: A survey. *International Journal of Advanced Robotic Systems, 10*(233), 1–9.

Brisilla, R., & Sankaranarayanan, V. (2015). Nonlinear control of mobile inverted pendulum. *Robotics and Autonomous Systems, 70*, 145–155.

Char, B.W., Fee, G.J., Geddes, K.O., Gonnet, G.H., & Monagan, M.B. (1986). A tutorial introduction to Maple. *Journal of Symbolic Computation, 2*(2), 179–200.

Charitos, T., de Waal, P.R., & van der Gaag, L.C. (2008). Computing short-interval transition matrices of a discrete-time Markov chain from partially observed data. *Statistics in Medicine, 27*(6), 905–921.

de Oliveira, E.C., & Machado, J. (2014). A review of definitions for fractional derivatives and integrals. *Mathematical Problems in Engineering, 2014*, 238459.

Dorčák, L. (1994). *Numerical models for the simulation of the fractional-order control systems* (Report No. UEF-04-94). Kosice, Slovak Republic: The Academy of Science, Institute of Experimental Physics. p. 1–112.

Fiori, S. (2008). Leap-frog-type learning algorithms over the Lie group of unitary matrices. *Neurocomputing, 71*(10), 2224–2244.

Gmiterko, A., & Grossman, M. (2010). *N*-link inverted pendulum modeling. In T. Brezina & R. Jablonski (Eds.), *Recent advances in mechatronics* (pp. 151–156). Berlin Heidelberg: Springer-Verlag.

Hedrih, K.R.S. (2008). Dynamics of multi-pendulum systems with fractional order creep elements. *Journal of Theoretical and Applied Mechanics, 46*(3), 483–509.

Higham, N.J. (2008). *Functions of matrices: Theory and computation*. Philadelphia, PA: SIAM.

Higham, N.J., & Lin, L. (2011). A Schur-Padé algorithm for fractional powers of a matrix. *SIAM Journal on Matrix Analysis and Applications, 32*(3), 1056–1078.

Housner, G.W. (1963). The behavior of inverted pendulum structures during earthquakes. *Bulletin of the Seismological Society of America, 53*(2), 403–417.

Ionescu, C.M. (2013). *The human respiratory system: An analysis of the interplay between anatomy, structure, breathing and fractal dynamics*. London: Springer-Verlag.

Israel, R.B., Rosenthal, J.S., & Wei, J.Z. (2001). Finding generators for Markov chains via empirical transition matrices, with applications to credit ratings. *Mathematical Finance, 11*(2), 245–265.

Jadlovská, S., Sarnovskỳ, J., Vojtek, J., & Vošček, D. (2015). Advanced generalized modelling of classical inverted pendulum systems. In P. Sinčák, P. Hartono, M. Virčíková, J. Vaščák, & R. Jakša (Eds.), *Emergent trends in robotics and intelligent systems* (pp. 255–264). Switzerland: Springer.

Kenneth, M., & Ross, B. (1993). *An introduction to the fractional calculus and fractional differential equations*. New York, NY: Wiley.

Kurdekar, V., & Borkar, S. (2013). Inverted pendulum control: A brief overview. *International Journal of Modern Engineering Research (IJMER), 3*(5), 2924–2927.

Larcombe, P. (1992). On the control of a two-dimensional multi-link inverted pendulum: The form of the dynamic equations from choice of co-ordinate system. *International Journal of Systems Science, 23*(12), 2265–2289.

Lewis, F.L., Dawson, D.M., & Abdallah, C.T. (2004). *Robot manipulator control: Theory and practice*. New York, NY: Marcel Dekker.

Lobas, L. (2005). Generalized mathematical model of an inverted multi-link pendulum with follower force. *International Applied Mechanics, 41*(5), 566–572.

Lopes, A.M., & Machado, J. (2014). Fractional order models of leaves. *Journal of Vibration and Control, 20*(7), 998–1008.

Lopes, A.M., Machado, J., Pinto, C.M., & Galhano, A.M. (2013). Fractional dynamics and MDS visualization of earthquake phenomena. *Computers & Mathematics with Applications, 66*(5), 647–658.

Luo, Y., & Chen, Y. (2012). *Fractional order motion controls*. Chichester: John Wiley & Sons.

Machado, J., & de Carvalho, J. (1989). Engineering design of a multirate nonlinear controller for robot manipulators. *Journal of robotic systems, 6*(1), 1–17.

Machado, J., de Carvalho, J., & Galhano, A. (1993). Analysis of robot dynamics and compensation using classical and computed torque techniques. *IEEE Transactions on Education, 36*(4), 372–379.

Machado, J., Kiryakova, V., & Mainardi, F. (2011). Recent history of fractional calculus. *Communications in Nonlinear Science and Numerical Simulation, 16*(3), 1140–1153.

Machado, J., Lopes, A.M., Duarte, F.B., Ortigueira, M.D., & Rato, R.T. (2014). Rhapsody in fractional. *Fractional Calculus and Applied Analysis, 17*(4), 1188–1214.

Mainardi, F. (2010). *Fractional calculus and waves in linear viscoelasticity: An introduction to mathematical models*. Singapore: World Scientific.

Mezić, I. (2006). On the dynamics of molecular conformation. *Proceedings of the National Academy of Sciences, 103*(20), 7542–7547.

Mitra, S.K., & Kuo, Y. (2006). *Digital signal processing: A computer-based approach* (Vol. 2). New York, NY: McGraw-Hill.

Moore, H. (2014). *MATLAB for engineers*. Upper Saddle River, NJ: Prentice Hall Press.

Papoulis, A. (1977). *Signal analysis* (Vol. 191). New York, NY: McGraw-Hill.

Petras, I. (2011). *Fractional-order nonlinear systems: Modeling, analysis and simulation*. Berlin Heidelberg: Springer-Verlag.

Podlubny, I. (1999). *Fractional differential equations*. San Diego, CA: Academic Press.

Rivas-Cambero, I., & Sausedo-Solorio, J.M. (2012). Dynamics of the shift in resonance frequency in a triple pendulum. *Meccanica, 47*(4), 835–844.

Schiehlen, W. (2014). On the historical development of human walking dynamics. In E. Stein (ed.), *The history of theoretical, material and computational mechanics – mathematics meets mechanics and engineering* (pp. 101–116). Berlin Heidelberg: Springer-Verlag.

Sheng, H., Chen, Y., & Qiu, T. (2011). *Fractional processes and fractional-order signal processing: techniques and applications*. London: Springer-Verlag.

Silva, M.F., Machado, J., & Lopes, A. (2004). Fractional order control of a hexapod robot. *Nonlinear Dynamics, 38*(1–4), 417–433.

Slotine, J.-J.E. (1985). The robust control of robot manipulators. *The International Journal of Robotics Research, 4*(2), 49–64.

Slotine, J.-J.E., & Li, W. (1991). *Applied nonlinear control* (Vol. 60). Englewood Cliffs, NJ: Prentice-Hall.

Spong, M.W., & Vidyasagar, M. (2008). *Robot dynamics and control*. New York, NY: John Wiley & Sons.

Valério, D., Trujillo, J.J., Rivero, M., Machado, J., & Baleanu, D. (2013). Fractional calculus: A survey of useful formulas. *The European Physical Journal Special Topics, 222*(8), 1827–1846.

Vesely, F.J. (2013). Of pendulums, polymers, and robots: Computational mechanics with constraints. *American Journal of Physics, 81*(7), 537–544.

Waugh, F.V., & Abel, M.E. (1967). On fractional powers of a matrix. *Journal of the American Statistical Association, 62*(319), 1018–1021.

Wolfram, S. (2000). *The mathematica book*. New York, NY: Cambridge University Press and Wolfram Research.

Yu, P., & Bi, Q. (1998). Analysis of non-linear dynamics and bifurcations of a double pendulum. *Journal of Sound and Vibration, 217*(4), 691–736.

Zayas, V.A., Low, S.S., & Mahin, S.A. (1990). A simple pendulum technique for achieving seismic isolation. *Earthquake Spectra, 6*(2), 317–333.